npj | biofilms and microbiomes

Article

Published in partnership with Nanyang Technological University

https://doi.org/10.1038/s41522-025-00750-6

A promiscuous Bcd amino acid dehydrogenase promotes biofilm development in *Bacillus subtilis*

David Ranava[1,9] ✉, Stephen M. Lander[2,3], Szu-Yu Kuan[1,4], Jonathan D. Winkelman[5], Arthur Prindle[1,2,6,7,8] & Mee-Ngan F. Yap[1] ✉

Glutamate dehydrogenase (GDH) resides at the crossroads of nitrogen and carbon metabolism, catalyzing the reversible conversion of L-glutamate to α-ketoglutarate and ammonium. GDH paralogs are ubiquitous across most species, presumably enabling functional specialization and genetic compensation in response to diverse conditions. *Staphylococcus aureus* harbors a single housekeeping GDH (GudB), whereas *Bacillus subtilis* encodes both a major and a minor GDH, GudB and RocG, respectively. In an unsuccessful attempt to identify an alternative GDH in *S. aureus*, we serendipitously discovered previously unrecognized GDH activity in two metabolic enzymes of *B. subtilis*. The hexameric Val/Leu/Ile dehydrogenase Bcd (formerly YqiT) catabolizes branched-chain amino acids and to a lesser extent glutamate using NAD^+ as a cofactor. Removal of *gudB* and *rocG* unmasks the dual $NAD(P)^+$-dependent GDH activity of RocA, which otherwise functions as a 3-hydroxy-1-pyrroline-5-carboxylate dehydrogenase. Bcd homologs are prevalent in free-living and obligate bacteria but are absent in most, if not all, staphylococci. Despite low sequence homology, Bcd structurally resembles the GudB/RocG family and can functionally compensate for the loss of GudB in *S. aureus*. Bcd is essential for the full maturation of biofilms. *B. subtilis* lacking GDHs exhibits severe impairments in rugose architecture and colony expansion of biofilms. This study underscores the importance of metabolic redundancy and highlights the critical role of substrate promiscuity in GDHs during biofilm development.

Glutamate dehydrogenases (GDHs) are housekeeping enzymes that connect nitrogen- and carbon-assimilation pathways by reversibly catalyzing the oxidative deamination of glutamate to produce α-ketoglutarate (α-KG) and ammonia using NAD^+, $NADP^+$ or dual NAD^+-$NADP^+$ as a cofactor. GDHs are widely distributed across eukaryotes and bacteria. They are classified by cofactor specificity[1,2] and further sub-grouped by protein molecular weights[3,4]. NAD^+-dependent GDHs, such as GudB enzymes from *Staphylococcus aureus* and *Bacillus subtilis*, are geared toward the catabolism of glutamate due to high Michaelis constant (K_m) for ammonia (Fig. 1a)[5]. By contrast, $NADP^+$-dependent GDHs predominantly proceed toward the reductive amination of ammonia. Small GDHs (S-GDH_{50} subfamily) in bacteria and eukaryotes generally adopt a homo-hexameric structure consisting of 45–50 kDa subunits, whereas large tetrameric GDHs (L-GDH_{115} and L-GDH_{180} subfamilies) in some bacteria and lower eukaryotes comprise 115–180 kDa protomers[3,4].

GDHs have significant physiological importance and biotechnological applications. Like other amino acid dehydrogenases, GDHs are catalysts for high-value amino acids used in the pharmaceutical and food and feed additives industries[6]. The GDH enzyme immunoassay (EIA) is a first-line diagnostic test for *Clostridioides difficile* infections due to the high

[1]Department of Microbiology-Immunology, Northwestern University Feinberg School of Medicine, Chicago, IL, 60611, USA. [2]Department of Biochemistry and Molecular Genetics, Northwestern University Feinberg School of Medicine, Chicago, IL, 60611, USA. [3]Medical Scientist Training Program (MSTP), Northwestern University Feinberg School of Medicine, Chicago, IL, 60611, USA. [4]Driskill Graduate Program (DGP), Northwestern University Feinberg School of Medicine, Chicago, IL, 60611, USA. [5]Trestle LLC, Milwaukee, WI, USA. [6]Department of Chemical and Biomedical Engineering, Northwestern University, Evanston, IL, 60208, USA. [7]Center for Synthetic Biology, Northwestern University, Evanston, IL, 60208, USA. [8]Chan Zuckerberg Biohub Chicago, Chicago, IL, 60642, USA. [9]Present address: Laboratoire de Bioénergétique et Ingénierie des Protéines, Institut de Microbiologie de la Méditerranée, CNRS, Aix-Marseille Université, 13009 Marseille, France. ✉e-mail: dranava@imm.cnrs.fr; frances.yap@northwestern.edu

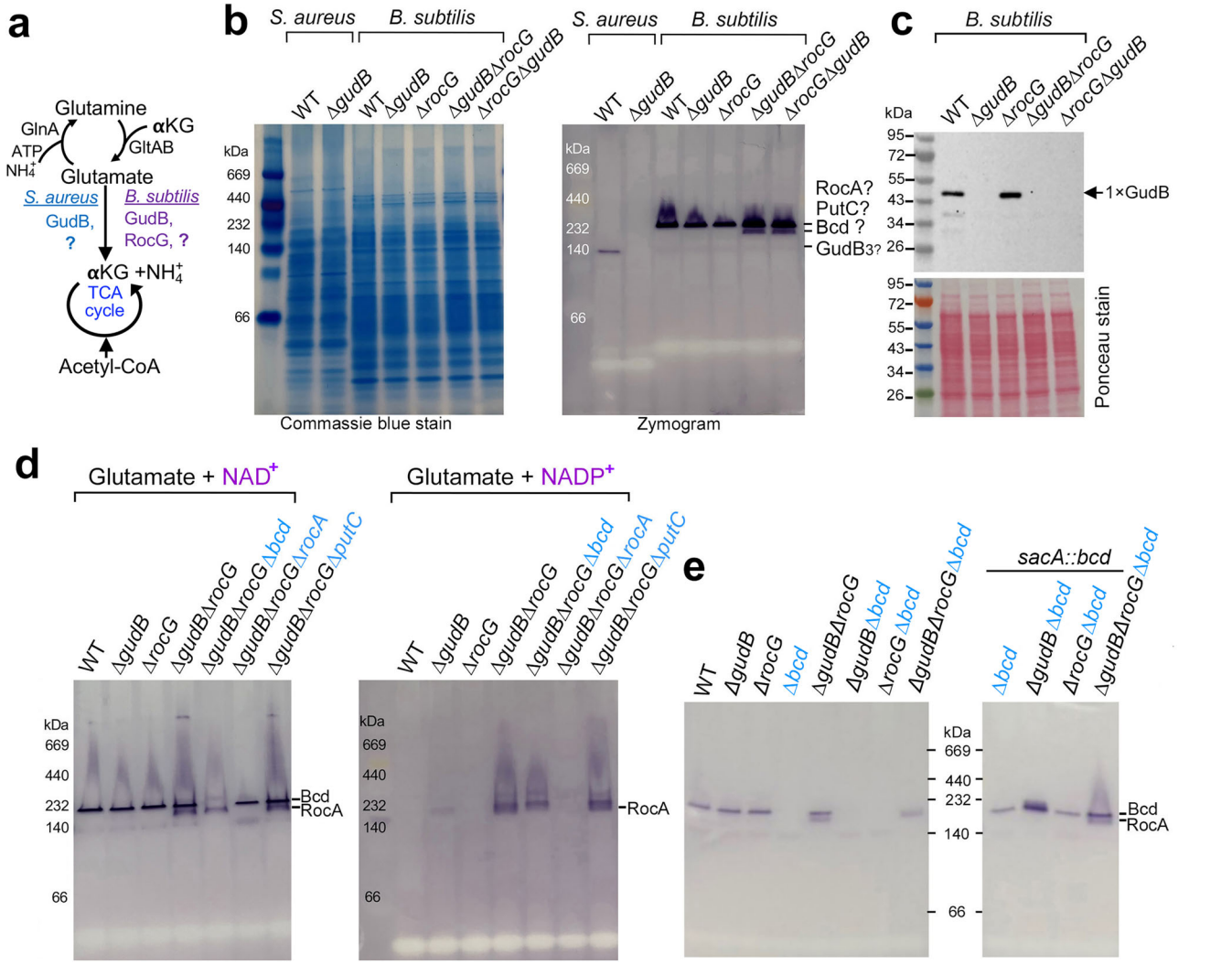

Fig. 1 | Bcd exhibits NAD^+-dependent GDH activity in wild-type (WT) *B. subtilis*, while RocA shows NAD(P)$^+$-dependent GDH activity only in the absence of GudB and RocG. a Simplified diagram of nitrogen and carbon metabolism in *S. aureus* and *B. subtilis*. The glutamate synthases GltA-GltB convert α-ketoglutarate (αKG) and glutamine into two molecules of glutamate. The glutamine synthetase GlnA catalyzes the ATP-dependent synthesis of glutamine from glutamate and ammonia. GudB and RocG deaminate glutamate to produce αKG, which feeds into the tricarboxylic acid cycle (TCA), generating acetyl coenzyme A (acetyl-CoA) through pyruvate oxidation. *B. subtilis* carries both GudB and RocG, while *S. aureus* harbors only GudB. Additional glutamate degrading enzymes (indicated by question marks) remain unidentified. **b** *B. subtilis* produces two additional GDHs of unknown identity, as revealed by in-gel activity staining. Independent double knockouts (Δ*gudB*Δ*rocG* and Δ*rocG*Δ*gudB*) show identical results. **c** Denaturing PAGE-immunoblot using the *B. subtilis* GudB antibody confirms proper *gudB* expression in the GudB-proficient strains. **d** Genetic knockouts confirm Bcd and RocA contributions to GDH activity. Both enzymes use NAD^+ as the coenzyme (left) but only RocA utilizes $NADP^+$ as the electron acceptor (right). **e** Zymogram analysis of a single *bcd* mutant and *bcd*-complemented strain rules out secondary mutations, substantiating Bcd as an alternative GDH. Zymography using NAD^+ and glutamate substrate is shown. GDH activity of GudB and RocG was not detected in this assay, possibly due to the sequestration of GudB by GltAB and low transcription of *rocG* in LB and MSgg media.

abundance of GDH in stool samples[7]. In bacteria, removing GDH leads to growth defects[8–12], aberrant biofilm development[13,14], attenuated virulence and host colonization[15–17], and sensitivity to antibiotic and environmental stress[17–20].

Enzyme promiscuity is central to metabolic diversity[21]. Duplication of GDH genes is well known in humans, yeast and bacteria. Human hGLUD1 and hGLUD2 differ significantly in tissue distribution and allosteric regulation[22]. In Firmicutes (synonym Bacillota), undomesticated *B. subtilis* strains, including NCIB3610, encode two functional GDH paralogs, GudB and RocG[5,23,24], which are differentially regulated[14,25]. However, laboratory strains of *B. subtilis*, such as strain 168, synthesize a non-functional GudB due to the insertion of an 18-bp long direct repeat in *gudB*, leading to the duplication of 3 amino acids in the active center of the GDH[5,23]. By contrast, GudB is the only GDH documented in the opportunistic pathogen *S. aureus* (Fig. 1a).

We previously reported that deletion of *gudB* in *S. aureus* does not completely abolish cellular GDH activity, suggesting the existence of a second GDH. We found that a 20 kDa protein of unknown function, YwlG, compensates for the loss of *gudB*, possibly by activating a hitherto unknown GDH (Fig. S1a)[26]. YwlG lacks the N-terminal and C-terminal substrate-binding domains and does not appear to possess intrinsic GDH activity, despite folding into a hexamer and structurally resembling the *B. subtilis* GudB[26,27]. Moreover, YwlG-dependent stimulation of cellular GDH is physically inhibited by a ribosome hibernation factor (Hpf). YwlG-Hpf sequestration reciprocally prevents the formation of ribonuclease-resistant, hibernating 100S ribosomes (Fig. S1a)[26]. We hypothesize that YwlG promotes cellular GDH activity by interacting with an unidentified protein in the absence of Hpf. In the process of identifying this unknown protein in *S. aureus*, we fortuitously discovered that an annotated Val/Leu/Ile dehydrogenase, Bcd in *B. subtilis* NCIB3610 displays a previously unrecognized

NAD^+-specific GDH activity. Even more surprisingly, deletion of both *gudB* and *rocG* unmasks the $NAD(P)^+$-dependent GDH activity of RocA, a 3-hydroxy-1-pyrroline-5-carboxylate dehydrogenase. Despite Bcd's absence in *S. aureus*, *B. subtilis* Bcd is functionally interchangeable with *S. aureus* GudB. In *B. subtilis*, deletion of *bcd* in combination with either *gudB* or *rocG* deletion impairs biofilm maturation. This study reveals the substrate promiscuity of amino acid dehydrogenases and suggests that many more redundant GDH enzymes remain to be discovered in all organisms.

Results

Discovery of two new glutamate dehydrogenases (Bcd and RocA) in *B. subtilis* NCIB3610

We employed an established native gel activity staining-based zymography approach[28,29] to identify the second GDH in total cell lysates of wild-type (WT) *S. aureus* and its Δ*hpf* null mutant. GDH activity was visualized by purple-stained protein bands, resulting from the dehydrogenase-mediated reduction of tetrazolium salts in the presence of glutamate substrate, a co-factor, and an electron carrier. In-gel zymography provides semi-quantitative and qualitative information about the native molecular weight of different GDH variants. Despite extensive experimental optimization and testing across multiple genetic backgrounds, we did not detect any GDH activity in *S. aureus* beyond the known GudB (Fig. S1b). Intriguingly, *S. aureus* GudB complexes migrate as a trimer (~ 135 kDa) on native PAGE, contrasting with the hexameric forms reported for other GudB homologs[14]. The identity of the trimeric GudB was confirmed by Western blots using a Δ*gudB* mutant as a control and a hexameric YwlG (~ 120 kDa) as the size marker (Fig. S1b). To rule out technical issues, we analyzed cell lysates from *B. subtilis* NCIB3610 LB or MSgg cultures as a control. On the zymogram, a GDH protein band corresponding to a hexameric GudB or RocG (~ 240 kDa) was detected in the zymogram. However, this multimer persisted upon *gudB* and *rocG* single deletion (Fig. 1b) and did not cross-react with the anti-GudB antibody, which recognizes both native and denatured GudB (Figs. S1c, and 1c). The absence of GudB activity in the WT *B. subtilis* is probably due to sequestration by GltA-GltB[13]. Further analysis of two independently constructed Δ*gudB*Δ*rocG* double knockouts revealed that the 240-kDa species was still present, along with an unexpected appearance of a lower molecular weight GDH band. These observations raised questions about the identities of the two protein species detected (Fig. 1b).

In-gel mass spectrometry analysis identified the lower band as either RocA or PutC, while the upper band corresponded to Bcd (Fig. S2). None of these proteins are previously known to exhibit GDH activity. RocA is a 56-kDa 3-hydroxy-1-pyrroline-5-carboxylate dehydrogenase, and PutC is a 56-kDa 1-pyrroline-5-carboxylate dehydrogenase. Both proteins can functionally replace each other in the utilization of proline and arginine[30]. Bcd, on the other hand, is a 40-kDa Val/Leu/Ile dehydrogenase[31], and its deletion triggers premature germination due to accumulation of valine[32]. Deletion of *bcd*, *rocA* and *putC* in the Δ*gudB*Δ*rocG* double mutant confirmed Bcd as the ~240-kDa complex and RocA as the smaller oligomer. Both proteins were able to use NAD^+ as the electron acceptor to degrade glutamate (Fig. 1d). RocA, but not Bcd, could also utilize $NADP^+$ as a cofactor; however, its GDH activity was only apparent in the absence of both GudB and RocG (Fig. 1d). A Δ*bcd* deletion mutant and its chromosomally encoded Bcd complement driven by its native promoter further validated the identity of the native Bcd complex (Fig. 1e). In summary, Bcd is an alternative NAD^+-dependent GDH enzyme in *B. subtilis*, and $NAD(P)^+$-dependent GDH activity of RocA is manifested in the absence of both GudB and RocG through an as-yet-unknown mechanism.

Recombinant Bcd forms a hexamer and exhibits Glu/Val/Leu/Ile dehydrogenase activities

B. subtilis Bcd migrates as a hexamer on native PAGE (Fig. 1) whereas *Lysinibacillus sphaericus* Bcd assembles as an octamer[33]. To confirm the oligomeric state and active form of Bcd, we recombinantly purified the N-terminally His-tagged WT Bcd protein and its catalytically compromised mutants (K68A, K80A, D115A) from *E. coli*. Only the WT and K80A variants were amenable to native purification (Fig. 2a, b). Both proteins eluted as hexamers on a size-exclusion chromatography (Fig. 2c, Data S1). Bcd is annotated as a branched-chain amino acid dehydrogenase. Using zymography and various L-amino acids as substrates, we confirmed that the recombinant WT Bcd exhibits NAD^+-dependent Val/Leu/Ile dehydrogenase activities and GDH activity in vitro. The K80A mutant showed a complete loss of dehydrogenase activity (Fig. 2d). Furthermore, in the presence of NAD^+ and L-glutamate, measurable catabolic GDH activity was detected in the hexameric WT Bcd fractions collected from the size-exclusion chromatography, relative to a $NAD(P)^+$-dependent bovine liver GDH control, whereas its Bcd(K80A) mutant had no activity (Fig. 2e). Similarly, untagged Bcd expressed in an *S. aureus* Δ*gudB* mutant demonstrated NAD^+-specific GDH and valine dehydrogenase activities (Fig. S3). These results demonstrate that the active form of *B. subtilis* Bcd is predominantly a hexamer capable of catabolizing multiple substrates.

The growth of the *B. subtilis*Δ*gudB*Δ*rocG* mutant is severely impaired in CE minimal medium containing glutamate as the sole carbon source[5,34]. We found that overexpression of Bcd, driven by a constitutive *rpsD* promoter, could partially restore the growth of the Δ*gudB*Δ*rocG* mutant to the level observed in the Δ*gudB* single mutant, although not to the levels of the WT or Δ*rocG* single mutant (Fig. 2f). This partial restoration of growth supports the involvement of Bcd in glutamate catabolism.

Bcd homologs are widespread across bacteria but absent in *S. aureus*

We next investigated the phylogeny and conservation of Bcd. Using OrthoFinder 2.5.5, we analyzed 136 bacterial genomes spanning a broad range of the bacterial clade within the tree of life. OrthoFinder identified hierarchical orthologous groups (HOGs), enabling the examination of orthology at various levels of the bacterial species tree. For example, a HOG at the root of the bacterial tree encompasses all genes descended from a single ancestral gene in the Last Bacterial Common Ancestor (LBCA). Conversely, a HOG at the *Bacillus* genus level includes all genes derived from the last common ancestor of all *Bacillus* species. At the root of the bacterial tree, RocG, GudB, and Bcd were grouped into a single HOG, suggesting they likely originated from a single ancestral gene near the LBCA. At the phylum level, Bcd was assigned to a distinct HOG (HOG_*bcd*) separate from GudB and RocG (HOG_*gudB/rocG*). GudB and RocG remained within the same HOG up to the species level, indicating a relatively recent divergence. Proteins from both HOG_*bcd* and HOG_*gudB/rocG* were identified in diverse bacterial phyla, with a notable absence of Bcd in most staphylococcal species, including *S. aureus*. The co-existence of *gudB/rocG* and *bcd* was common in *Bacillus* sp, *Bdellovibrio* sp., *Halalkalibacterium* sp., and *Deinococcus* sp. Additionally, *bcd* was prevalent in pseudomonads and obligate pathogens (Fig. 3a, Data S2).

To further explore Bcd orthology. We expanded our analysis to 26,373 genomes from the ProGenomes database[35], which provides a non-redundant collection of high-quality genomes, each representing a single SpecI species cluster. A reciprocal BLAST approach was employed using Bcd from *B. subtilis* as the query in a forward BLASTp against all proteomes. The top hit from each target proteome was subsequently blasted back against the *B. subtilis* genome. If the Bcd query protein emerged as the best hit in the reciprocal BLAST, the corresponding target proteome hit was designated as a putative Bcd ortholog. Consistent with the initial analyses, Bcd homologs were predominantly found in the phyla Bacillota, Gemmatimondota, Bacterioidota, Pseudomonadota, Bdellovibrionota, Deinococcota, Myxococcota, and Chlamydiota, particularly in bacteria with free-living and obligate lifestyles (Fig. 3b).

B. subtilis Bcd rescues the growth defects of an *S. aureus* Δ*gudB* mutant

Bcd shares only 27–28% overall protein sequence identity with GudB and RocG, which is significantly lower than the identity between GudB

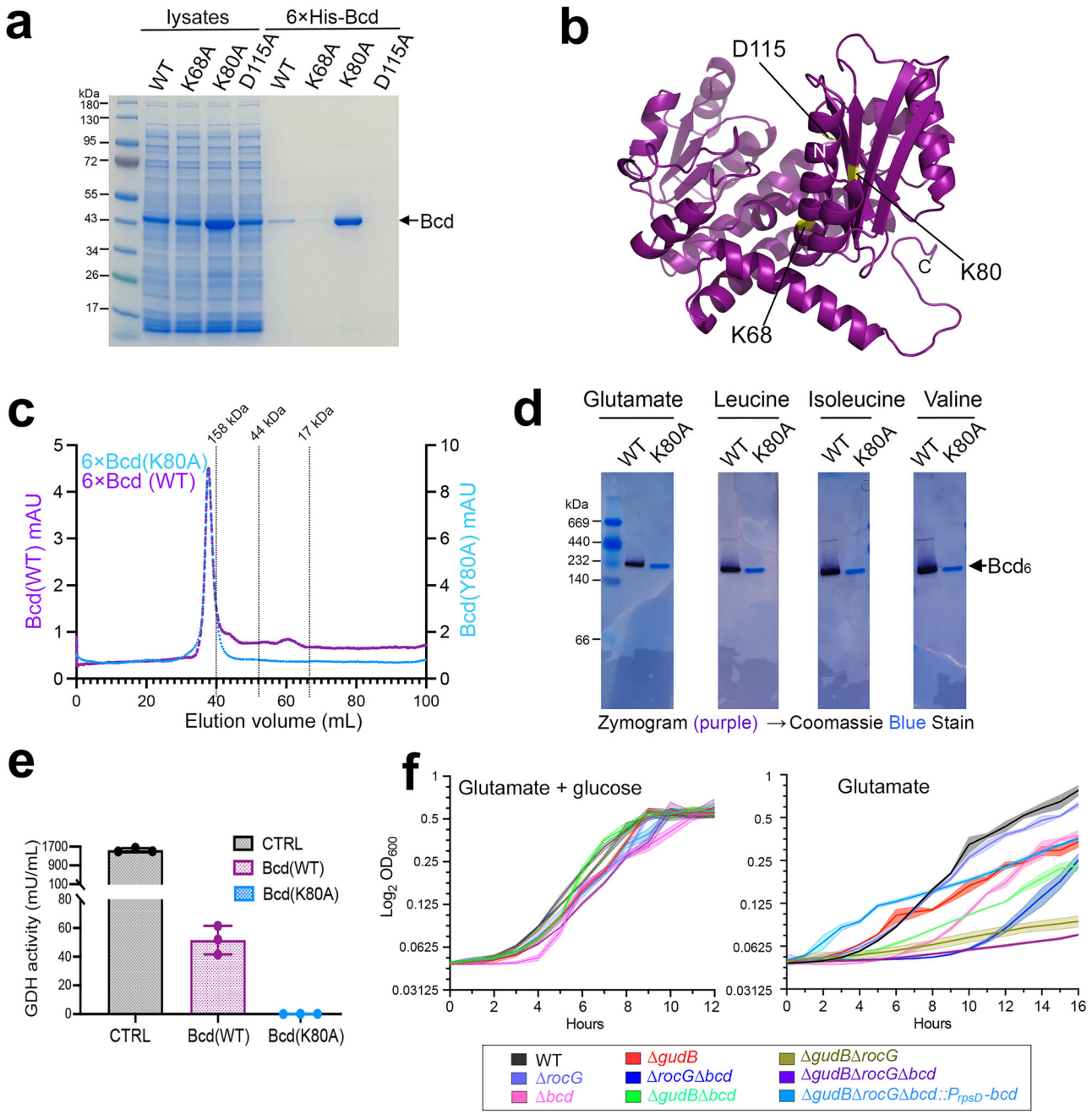

Fig. 2 | In vitro characterization of Bcd. a Recombinant WT Bcd and its catalytically impaired mutants were purified by cobalt TALON affinity chromatography. **b** Structural prediction of Bcd monomer by Alphafold shows the catalytic sites. **c** WT Bcd and its K80A mutant form a hexameric assembly, as observed in size-exclusion chromatography. **d** Zymography shows that WT Bcd exhibits Glu/Val/Leu/Ile dehydrogenase activity, while the K80A mutant is catalytically inactive despite forming a hexamer. Zymograms followed by Coomassie Blue staining show equal loading and differing GDH activity. **e** In vitro GDH activity of purified Bcd hexamers collected from (**c**). WT Bcd exhibits measurable GDH activity, though significantly lower than that of the commercially available NAD(P)$^+$-dependent bovine liver GDH control (CTRL). **f** Growth kinetics of *B. subtilis* mutants in CE minimal medium containing glucose and glutamate or glutamate alone as the carbon and nitrogen source. The Δ*gudB*Δ*rocG* double and Δ*gudB*Δ*rocG*Δ*bcd* triple mutants grew poorly due to their inability to utilize glutamate. Overexpression of *bcd* partially rescues this growth defects. Color-coded traces represent the mean OD_{600} and shaded areas indicate the standard deviation from three independent biological replicates.

and RocG (74–75%). At the structural levels, Alphafold modeling[36] showed that *B. subtilis* Bcd is nearly identical to *S. aureus* GudB, with a root mean square deviation (r.m.s.d) of 1.49 Å (Fig. 3c). Plasmid-borne expression of Bcd restored the cellular GDH activity in the *S. aureus* Δ*gudB* mutant, although not to the levels achieved by expressing the cognate GudB (Fig. 3d). The *S. aureus* Δ*gudB* exhibits growth defects under various laboratory conditions, including lysogeny broth (LB) medium[8,9]. GudB is essential for growth following glucose consumption. A Δ*gudB* mutant prematurely enters stationary phase upon glucose depletion due to its inability to utilize glutamate as an alternative carbon source[8]. Indeed, we observed that deletion of *gudB* significantly hindered *S. aureus* growth in LB. These growth defects were fully complemented by plasmid-based expression of either the cognate GudB or heterologous *B. subtilis* Bcd (Fig. 3e). The modest difference observed between the GudB-complemented (blue trace) and Bcd-complemented (orange trace) strains during stationary phase may

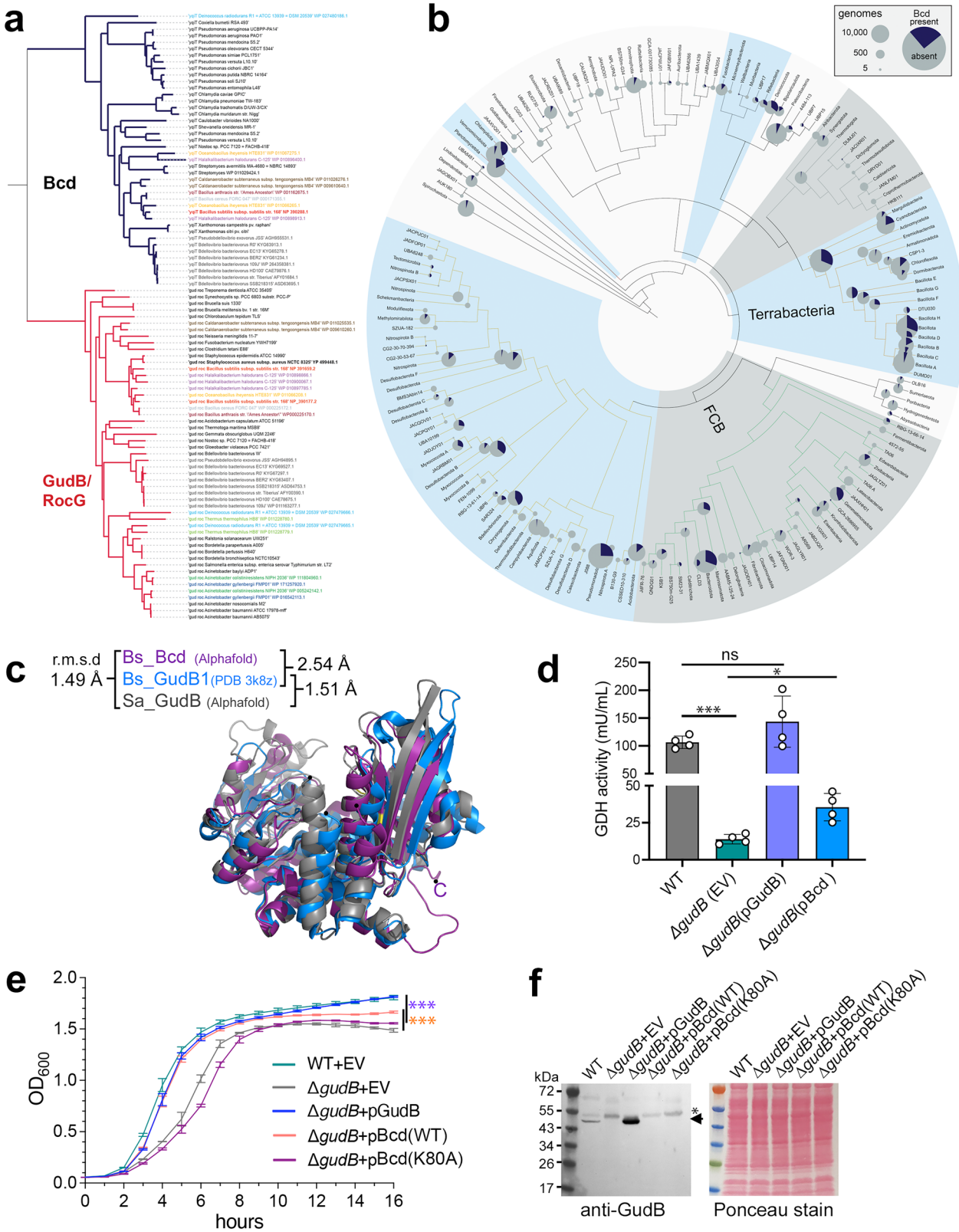

be partially due to the lower GDH activity of Bcd compared to GudB (Fig. 3d) to efficiently use glutamate as an alternative carbon source, leading to carbon limitation. In contrast, a catalytically inactive Bcd(K80A) failed to restore growth to the WT level (Fig. 3e, f). These findings confirm that *B. subtilis* Bcd can functionally replace *S. aureus* GudB in glutamate degradation.

Bcd is required for biofilm maturation in *B. subtilis*

The homeostasis of glutamate, glutamine and ammonium is known to regulate biofilm development[11,13,37–39]. Gradients of glutamate and ammonium influence the oscillatory dynamics of biofilm expansion through GDH-dependent ammonium synthesis within the interior of the colony, utilizing glutamate diffused from the periphery (Fig. 4a, left panel)[37,38]. To

Fig. 3 | *B. subtilis* Bcd functionally substitutes for the loss of GudB in *S. aureus*, which lacks a Bcd homolog. a Phylogenetic tree shows that Bcd and GudB/RocG form two monophyletic clades. Multiple Bcd and GudB/RocG paralogs can be found in a single species, e.g., *H. halodurans*, which are color-coded accordingly. **b** Taxonomic distribution of Bcd homologs. The pie-chart size and black section represent the number of bacterial genomes and the frequency of Bcd presence, respectively. Terrabacteria mostly include Gram-positive bacteria such as Bacillota (Firmicutes); FCB phylum consists of Fibrobacteriota, Chloraobiota, and Bacteriodota. Less well-defined superphyla are loosely categorized by color. **c** Structural superposition of *B. subtilis* GudB1 structure (PDB 3k8z) with predicted structures of *B. subtilis* Bcd and *S. aureus* GudB reveals high resemblance among these GDHs. **d** Plasmid borne-Bcd partially restores GDH activity in a *S. aureus ΔgudB* mutant. EV, empty vector. Statistical significance was determined using Student's t-test. $^{*}P < 0.05$, $^{***}P < 0.001$, ns = not significant. **e** Growth defects of the *S. aureus ΔgudB* mutant are fully complemented by WT Bcd and its cognate GudB but not by the Bcd(K80A) mutant. Student's *t*-test ($n = 4$), $^{***}P < 0.001$. **f** Western blot analysis shows endogenous GudB and plasmid-borne GudB expression in *S. aureus*. Anti-GudB does not cross-react with Bcd despite structural similarity. An asterisk indicates non-specific band.

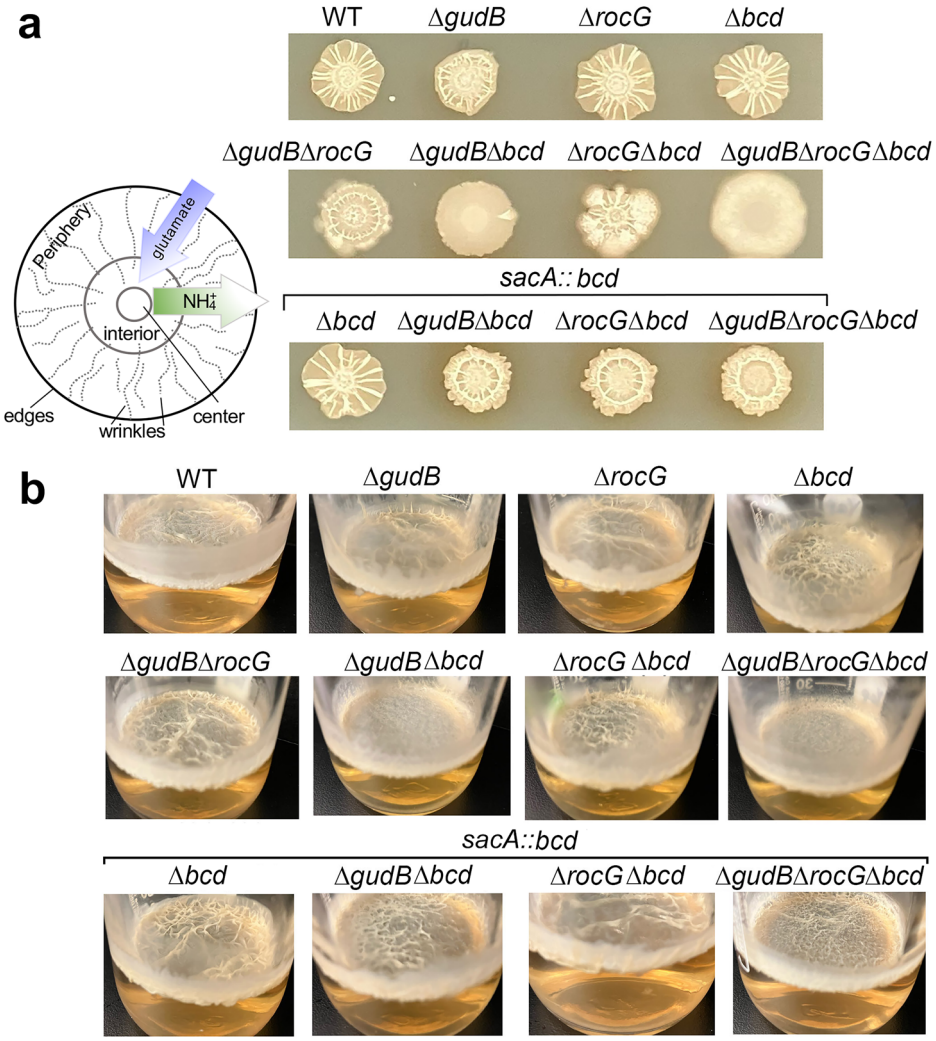

Fig. 4 | Glutamate homeostasis is essential for biofilm development in *B. subtilis*. a Inactivation of the major GDH (GudB) and Bcd abolishes the wrinkled morphology of biofilm colonies. Removing *gudB*, *rocG* and *bcd* together results in aberrant biofilm expansion. (Left) A schematic of glutamate metabolism shows that biomass production requires external glutamate and ammonium generated internally via GDH-mediated glutamate degradation. **b** Pellicle biofilms at the air-liquid interface lose their rugose structures in the absence of GudB and Bcd. These defects are exacerbated in the Δ*gudBΔrocGΔbcd* triple mutant. Chromosomal expression of *bcd* from the *sacA* locus under its native promoter provides varying degrees of complementation in different mutants.

investigate the role of Bcd in biofilm formation, we examined the morphological and structural changes of colony biofilm on solid agar and floating pellicle biofilm at the air-liquid interface. Under biofilm-inducing conditions[40], *B. subtilis* NCIB3610 forms rugose colony biofilms on LBGM agar, characterized by concentric rings of cell differentiation. Wrinkles form as a consequence of localized cell death, coupled with the stiffness and hydrophobicity provided by the exopolysaccharides- and proteins-containing extracellular matrix[41]. All mutant strains, with the exception of the Δ*rocGΔbcd* mutant, displayed comparable growth in LBGM medium relative to the WT (Fig. S4). GudB and RocG are considered major and minor GDH in strain NCIB3610, respectively. While the single Δ*bcd* mutant did not exhibit measurable defects in macrocolony formation, combining the Δ*bcd* deletion with Δ*gudB* deletion completely abolished the rugose architecture of the colonies. Additionally, combining Δ*bcd* deletion with Δ*rocG* deletion modestly altered the corrugated surface of the colonies. A triple mutant (Δ*gudBΔrocGΔbcd*) not only abolished the wrinkly morphology but also exhibited dysregulated colony expansion. In general, biofilm phenotypes were more pronounced when both *gudB* and *bcd* knockouts were combined. The chromosomally encoded *bcd* from the *sacA* locus fully restored the rugose texture and corrected colony expansion of the triple mutant, but only partially restored radial patterns to WT levels (Fig. 4a). Frilled colony and appendage-like cell growth were observed at the edges of colonies in the Δ*gudBΔrocG* and Δ*rocGΔbcd* double mutants, suggesting the emergence of suppressors, which are commonly found in *gudB* and *rocG* mutants[5,34,42]. In line with the colony biofilm phenotype, the Δ*gudBΔbcd and* Δ*gudBΔrocGΔbcd* mutants were impaired in forming the corrugated architecture in the pellicle, instead producing a powdery texture that could be complemented by chromosomally encoded *bcd* (Fig. 4b). Bcd likely plays a secondary role in glutamate degradation (Fig. 2d-2f) and Val/Leu/Ile dehydrogenase activity of Bcd may partially contribute to the

observed phenotypes. Nevertheless, the biofilm phenotypes confirm the functional redundancy of Bcd, GudB and RocG in glutamate degradation, highlighting the importance of GDH activity in biofilm development.

Discussion

Here we report a novel dehydrogenase activity for NAD^+-specific Val/Leu/Ile dehydrogenase (Bcd/YqiT) in deaminating glutamate. We also identify a previously unrecognized $NAD(P)^+$-dependent GDH activity of RocA, which is revealed when both *gudB* and *rocG* are deleted. The *B. licheniformis* RocA homolog (PDB 3RJL), a 3-hydroxy-1-pyrroline-5-carboxylate dehydrogenase, is structurally distinct from Bcd, GudB, and RocG. The additional GDH activity of RocA represents a new example of compensatory redundancy. Genetic compensation can also occur by establishing a new pathway to restore glutamate degradation through the overexpression of aspartase AnsB, allowing the Δ*gudB*Δ*rocG* double mutant to feed glutamate into the TCA cycle[25,43]. Furthermore, a loss-of-function mutation in the glutamate synthase *gltB* of the Δ*gudB*Δ*rocG* double mutant also prevents glutamate accumulation[5].

Glutamate is one of the most abundant cytoplasmic anions and the major nitrogen reservoir in bacteria, with cellular concentrations reaching up to 150 mM[44]. Glutamate stabilizes interactions among biomolecules, acts as a counterion to potassium, buffers intracellular pH, maintains osmolarity, and serves as an amino group donor for at least 37 transamination reactions[13,44–46]. Glutamate overload is toxic for *B. subtilis* under conditions of GDH deficiency and excessive glutamate uptake and synthesis[5,42,47]. GudB and RocG, and to a lesser extent, Bcd and RocA are metabolically redundant in degrading glutamate, ensuring robustness against fluctuations in glutamate and *gdh* mutations. *B. subtilis gudB* is constitutively expressed, while *rocG* expression is repressed by glucose and activated by arginine[14]. *gudB*, *rocG*, *bcd*, and *rocA* are differentially expressed under various conditions[14,31,48,49], allowing fine-tuned glutamate catabolism based on cellular needs.

GudB, RocG, Bcd and RocA are multi-tasking enzymes, performing regulatory role in addition to degrading multiple substrates. GudB and RocG act as trigger enzymes that not only carry GDH activity but also directly interact with the GltC transcription factor to regulate glutamate[25,48,50,51] synthesis. RocA recognizes both L-glutamate 5-semialdehyde and L-glutamate substrates and uses NAD^+ and $NADP^+$ as electron acceptors. Bcd degrades branched-chain amino acids as well as glutamate (Fig. 2), with Bcd-mediated valine catabolism regulating the timing of germination in *B. subtilis*[32]. Our phylogenetic analysis suggests that the *gudB/rocG* and *bcd* clades may have diverged evolutionarily to expand their substrate repertoire (Fig. 3). Notably, combinations of point mutations in the substrate-binding pocket of leucine dehydrogenase and GDH can switch amino acids specificity in vitro[52–54]. The prevalence of Bcd in intracellular pathogens and bacteria inhabiting diverse aquatic and terrestrial environments suggests a selective growth advantage due to substrate ambiguity in these niches.

Niche specialization of GDH could partially explain our inability to identify a second GDH in *S. aureus*. The expression and activity of this alternative GDH in *S. aureus* may be too low[14], inhibited by other factors[13], or inactivated by post-translational modifications[55] under the conditions we tested. For instance, *B. subtilis* GudB activity is repressed by the heterodimeric GltAB in non-fractionated samples, and *rocG* is normally transcriptionally repressed[13], which may account for the absence of GudB- and RocG-mediated GDH activity on the zymograms (Fig. 1). Zymography has inherent limitations[28], such as resolution and sensitivity issues, and our current electrophoresis protocols preclude the detection of multimer larger than 1200 kDa, such as the 1.6 MDa GltAB-GudB complex. Moreover, GltAB-GudB interaction inhibits GudB activity, potentially explaining a lack of GudB's GDH activity on the zymogram from LB and Msgg cultures.

Mutations in *gudB* impair colony biofilm formation[11,13,14]. Consistent with previous reports, a Δ*gudB* mutant exhibits modest but measurable biofilm developmental defects. We find that inactivating both *bcd* and *gudB* severely diminishes the rugose phenotype, and inactivating all three GDHs produces rapidly growing smooth colonies (Fig. 4). These additive biofilm defects confirm the overlapping role of GudB, RocG and Bcd. GDH activity may influence biofilm maturation in multiple ways: (i) Biofilm oscillations are beneficial for cells to cope with nutrient deprivation and chemical stress. GDH insufficiency disrupts normal growth oscillations, which involve gradients of glutamate and ammonium[37,38,56]. (ii) Acidic and alkaline conditions hinder biofilm formation[57]. GDH deficiency can lead to high glutamate and low pH. (iii) Unlike strain B1, whose biofilm matrix is primarily composed of hydrophilic poly-γ-glutamate (γ-PGA), NCIB3610's matrix contains very little γ-PGA[58,59]. However, the possibility that GDH deficiency increases γ-PGA levels and alters biofilm architecture cannot be entirely excluded.

Methods

Bacterial strains, plasmids, primers and chemicals

Strain USA300 JE2 is a community-associated methicillin-resistant *Staphylococcus aureus* (CA-MRSA, GenBank CP000255). The JE2 mutant derivatives carry a *bursa aurealis* transposon insertion were acquired from ATCC-managed BEI Resources Repository and were backcrossed to isogenic JE2 background by Φ11 phage transduction[60]. The in-frame Δ*gudB*::Km deletion mutant was created using standard allelic-exchange recombination[61]. A 2-kb flanking region of *S. aureus gudB* (locus SAUSA300_0861) was PCR amplified with the primer pairs P1747/P1748 and P1749/P1750 via 2-step PCR using JE2 genomic DNA as the template. The product was digested with SacI and SalI and cloned into the same sites of pBT2. The resulting pBT2Δ*gudB* was digested with SmaI, dephosphorylated, and ligated to the blunt-ended 1.6-kb kanamycin (Km) resistance cassette that was released and end-repaired from pBTK by KpnI and PstI digestion. The resulting construct pBT2Δ*gudB*::Km was propagated in *E. coli* DC10B, and the plasmid reisolated, electroporated into JE2 and selected at 30 °C on agar plates supplemented with 10 μg/mL chloramphenicol. The integrant was further selected by a 43 °C temperature upshift on chloramphenicol-containing agar plates. The homologous recombinant was resolved by 30 °C passages and cycloserine enrichment following the published procedures[62]. Mutant strains were verified by Sanger sequencing and Western blots.

Restriction-free cloning was used to construct pEPSA5_GudB, pEPSA5_Bcd, and pMCSG7 derivatives[63]. To construct N-terminally His-tagged *bcd* for protein purification, primers P2139/P2140 were used to assemble the DNA fragment onto pMCSG7. Primers used to construct pEPSA5_GudB and pEPSA5_Bcd were P1753/P1754 and P2130/P2131, respectively. Site-directed mutagenesis was performed using Quikchange mutagenesis kit (Agilent Genomics) using P2133/P2134 (K68A), P2135/P2136 (K80A), and P2137/P2138 (D115A).

B. subtilis NCIB3610 (ATCC 6051 or DSM10, GenBank CP020102) is an undomesticated biofilm former that is poorly competent[24,64]. Gene deletions mutants in NCIB3610 were made using phage transduction and a commercially available gene knockout library in *B. subtilis* 168[65,66]. SPP1 phage transduction was completed by moving gene knockouts from the donor 168 strain into the receiving NCIB3610 strain as described in detail previously[67]. Double mutants were made by utilizing the Cre recombinase recognition sites, *loxP*, built into the commercially available gene knockout library that allowed for removal or curing of the antibiotic cassette[65]. To remove the antibiotic cassette, the strain was transformed with a temperature sensitive plasmid that contained a constitutively expressed Cre recombinase using the previously described transformation method for NCIB3610 with all incubation steps carried out at 30 °C[68]. The curing of the antibiotic cassette was then completed using the described procedure[65]. Cured mutants were then used as the recipient strain for sequential phage transduction. All genotypes were confirmed with specific flanking primers for all genes and Sanger sequencing.

All strains, oligos and plasmids are listed in Tables S1-S2. Unless otherwise noted, *S. aureus* cells were grown aerobically at 37 °C in tryptic soy broth (TSB, BD Difco #211822), Msgg [5 mM potassium-phosphate buffer (pH 7) 100 mM MOPS, 2 mM $MgCl_2 \cdot 6H_2O$, 700 μM $CaCl_2$, 50 μM $MnCl_2$,

100 μM $FeCl_3 \cdot 6H_2O$, 1 μM $ZnCl_2$, 2 μM thiamine-HCl, 0.5%(v/v) glycerol, 0.5% (w/v) monosodium glutamate][69] or Lysogeny Broth (LB, BD Difco #244610) at a 5:1-10:1 tube- or flask-to-medium ratio with a 1:100 dilution of an overnight seed culture. *B. subtilis* and *E. coli* were grown in LB. When necessary, erythromycin, chloramphenicol, kanamycin, ampicillin, xylose, IPTG were used at 5 μg/mL, 10 μg/mL (7.5 μg/mL in *B. subtilis*), 75 μg/mL (10 μg/mL in *B. subtilis*), 100 μg/mL, 10 mM, and 0.5 mM, respectively. Unless otherwise noted, all chemicals and oligonucleotides were purchased from Millipore Sigma-Aldrich and IDT DNA, respectively.

Chromosomal *bcd* complementation

The constitutively expressed *rpsD* promoter-driven Pc-bcd plasmid and native promoter-driven Pn-*bcd* plasmid were constructed by amplifying 500-bp of the *rpsD* or operonic *bkdR-ptb-bcd* promoters from the NCIB3610 genome and assembled onto pSac-Cm (or ECE174) using a restriction-free cloning method[63,69]. Primers used for the assembly were P2149/P2150 and P2154/P2155 (Table S2). The assembled plasmids were transformed into and integrated into NCIB3610 *sacA* locus using a natural competence protocol previously established[68]. Transformants were selected on LB agar containing 7.5 μg/mL chloramphenicol. Low efficiency of transformation was achievable despite the presence of ComI-containing plasmid pBS32 in the parental NCIB3610 strain[68], which was verified by whole-genome sequencing. All genotypes were confirmed with specific flanking primers on *sacA* and *bcd* sequences.

His-tag affinity purification of Bcd recombinant proteins and size-exclusion chromatography

Overnight *E. coli* seed cultures were diluted 1/100-fold in 200 mL LB supplemented with 100 μg/mL ampicillin and incubated at 37 °C until to an OD_{600} = 0.5–0.6. Cells were induced with 0.5 mM IPTG for 3-4 hr. Then cultures were centrifuged at 3220×*g* for 15 min at 4 °C to pellet cells. Supernatant was discarded, and cells were resuspended in 5 mL of Buffer I (50 mM Tris-Cl (pH 7.5), 150 mM NaCl, 1 mM phenylmethylsulfonyl fluoride (PMSF)) containing 1 mM imidazole and lysed on a FastPrep-24 instrument using Lysing Matrix B beads (MP Biomedicals # 116911500). Following lysis, samples were centrifuged at 4 °C, 20,817×*g* for 5 min to remove cell debris. Approximately 5 mL of cell lysates was incubated with 0.5 ml TALON metal affinity beads (Takara, #635503) on a tube rotator at 4 °C for 1 hr. The column was washed extensively with Buffer I supplemented with 20 mM imidazole (7 ×1 mL), and proteins were eluted with Buffer I supplemented with 50–300 mM imidazole.

For size-exclusion chromatography, approximately 1.8 mg of Bcd(WT) and 2 mg of Bcd (K80A) proteins were loaded on HiPrepTM 16/60 Sephacryl S-100 HR column (Cytiva) on an ÄKTA Go chromatography system (Cytiva) and equilibrated with Buffer II [50 mM Tris-Cl (pH 7.5), 150 mM NaCl][70]. To estimate the size of Bcd peaks a Gel Filtration Standard (BioRad #151-1901) was used.

Zymography and in-gel mass spectrometry

Zymography was performed following the published protocol[29]. Fifty microliters of overnight cultures were diluted in 25 ml of LB or Msgg (*B. subtilis*) and TSB (*S. aureus*). The cultures were grown for 24 h at 37 °C and 10 mL of culture were centrifuged at 3220×*g* for 15 min at 4 °C. Cell pellets were resuspended in 1 ml of sterile water and lysed on a FastPrep-24 instrument using Lysing Matrix B beads (MP Biomedicals). Following lysis, samples were centrifuged at 20,817×*g* at 4 °C for 5 min. Fifty microliters of the cell-free extracts were mixed with equal volume of 2×Native Sample Buffer (Invitrogen, catalog # LC2673) and 10 μl were analyzed on a 4–12% Tris-glycine native gel (Invitrogen #XP04122BOX) in Tris-Glycine Native Running Buffer (Invitrogen #LC2672) at constant 200 V for 80 min. The gels were rinsed in ddH_2O for 5 min before incubation in 30 ml activity solution in the dark for 1 hr or overnight at 37 °C. The activity solution comprised of 0.5 mM $NADP^+$ (Sigma #10128031001) or NAD^+ (Sigma #NAD100-RO), 50 mM Tris-HCl (pH 8.0), 20 mM L-glutamate (Sigma #49601-100 G), 0.3 mg/ml Nitro Blue Tetrazolium (Sigma #N5514-10TAB), and 0.05 mg/mL phenazine methosulfate (Sigma #P9625-1G). For Leu/Val/Ile dehydrogenase activity, L-glutamate was substituted with 20 mM L-valine (Sigma #V0500-100G, L-leucine (Sigma #L8000-100G) or L-isoleucine (Sigma #I2752-100G). Dehydrogenase activity appeared as a dark purple against a clear background after extensive wash in ddH_2O to remove residual yellow dyes. The gels were subsequently stained with Gelcode Blue Safe Stain (ThermoFisher #PI24956) to ensure equal loading. A HMW Native protein marker kit (Cytvia #17044501) was used to estimate Bcd or GudB oligomerization. For mass spectrometry, protein bands of interest were excised from the zymogram gel and subjected to in-gel trypsin digestion at 37 °C. Digested peptides were extracted with trifluoracetic acid (TFA) extraction buffer, desalted by passing through the C-18 Zip-tips[71]. The digested peptides were then separated on a nano-flow Ultimate 3000 and analyzed by Orbitrap Exploris high-resolution mass spectrometer. Protein identification using Nano LC-MS/MS was performed by Applied Biomics (Hayward, CA)

In vitro glutamate dehydrogenase (GDH) assays

GDH Activity Assay was performed as previously published[26]. Briefly, *S. aureus* and *B. subtilis* were grown aerobically in 25 ml of TSB and LB, respectively for 24 h at 37 °C. One milliliter of bacterial cultures was collected, resuspended in sterile water, and lysed on a FastPrep-24 instrument using Lysing Matrix B beads (MP Biomedicals), and 10 μL cell lysates were immediately used in the reactions. GDH activity was measured by the amount of NADH production upon glutamate consumption using a colorimetric (450 nm) kit according to manufacturer's procedures (Abcam # ab102527 or Sigma #MAK099). To determine GDH activity of the purified proteins, 4.5 μM of Bcd proteins and 0.8 μM of positive control bovine liver GDH (Sigma #G2626) were used. One unit of GDH is defined as the amount of enzyme that generates 1.0 μmol of NADH per minute at pH 7.6 at 37 °C.

Native Gel immunoblots

Fifteen microliters of the cell-free extracts prepared as described in "Zymography" were analyzed on a 4–12% Tris-glycine native gel (Invitrogen). Proteins were transferred onto a 0.22 μm PVDF membrane (Bio-Rad #1704156) using a Trans-Blot Turbo Transfer System (Bio-Rad). Membranes were immunolabelled using epitope-specific rabbit polyclonal anti-$GudB_{Bs}$ (1/1,000 dilution)[13] and anti-YwlG (1/4000 dilution)[26]. HRP-conjugated anti-IgG secondary antibody (1/15,000 dilution) was from Cytiva (#NA9120) and SuperSignal™ West Dura chemiluminescence substrate (Thermo Scientific #34075) was used for signal detection. Images were acquired using iBright FL1500 system (ThermoFisher).

Phylogenetic analysis

To determine orthologous relationships between Bcd, RocG and GudB, we used OrthoFinder version 2.5.5[72] to analyze 136 bacterial genomes representing a wide span of the bacterial clade in the tree of life. A phylogenetic tree was constructed using all proteins from both *bcd*-HOG and *gudB/rocG*-HOG. Amino acid sequences were aligned with MUSCLE 5.1 using default settings, and an unrooted tree was inferred with FastTree version 2.1.11.

The analysis of *bcd* orthology was expanded to 26,373 genomes from the ProGenomes database. This dataset comprises a non-redundant collection of high-quality genomes, with one representative genome for each SpecI species cluster. A reciprocal BLAST approach was employed, using *bcd* from *Bacillus subtilis* 168 as the query in a forward BLASTp against all other proteomes. The top hit from each target proteome was subsequently blasted back against the *Bacillus subtilis* genome. If the *bcd* query protein was identified as the best hit in the reciprocal BLAST, the corresponding target proteome hit was designated as a putative *bcd* ortholog. Custom python scripts were used to run and analyze results from Orthofinder and reciprocal blast and are available on GitHub at https://github.com/JonWinkelman/reciprocal-blast (Trestle Biosciences, LLC). Interactive Tree of Life (iTol) tool and Adobe Illustrator were used for visualizing and annotating phylogenetic trees.

In silico analyses

The predicted structures for *S. aureus* GudB and *B. subtilis* Bcd were made using AlphaFold 3[73] and rendered with PyMOL Molecular Graphics System (version 3.0 Schrödinger, LLC), yielding a per-residue model confidence score (pLDDT) of >70–90 and >90 for GudB and Bcd, respectively. To discern relationships to known structures, the predicted structures were submitted to the DALI server (v5)[74] to compare against available structures.

Biofilm assays and growth kinetics

Assays of biofilm formation were adapted from refs. 40,75. Single colonies of *B. subtilis* strains were cultured overnight in 3 mL of LB medium at 37 °C. The seed cultures were diluted in fresh 25 ml LB supplemented with 0.1 mM $MnSO_4$•$4H_2O$ and 3% (v/v) glycerol (LBGM) to an OD_{600} of 0.1. To induce pellicle formation, 20 mL subculture were transferred to sterile 50-ml Pyrex bottles and incubated at 25 °C without agitation for 48 h before the images were recorded. For colony biofilm formation, 2 µL of the OD_{600} 0.1 cultures were spotted onto the LBGM agar. Plates were incubated at 37 °C for 24 h prior to imaging. All experiments were repeated at least three times.

For growth kinetics, strains were grown to OD_{600} 0.8-1.0 in LB, spun down, resuspended in 1×PBS and adjusted to OD_{600} 0.8. Two microliters of cell suspension were seeded into 200 µL of CE minimal medium, LB, or LBGM[40] in a 96-well microplate. Bacterial growth was recorded at 37 °C with 150 rpm shaking on a TECAN SPARK multimode plate reader equipped with a humidity cassette. The CE minimal medium comprises [70 mM K_2HPO_4, 30 mM KH_2PO_4, 25 mM $(NH_4)_2SO_4$, 0.5 mM $MgSO_4$, 10 µM $MnSO_4$, 50 mg/L tryptophan] with and without 1 g/L glucose and 8 g/L potassium glutamate[5].

Statistical analysis

Statistical analyses were performed using GraphPad Prism 10.1.1. The performed statistical tests are described in the figure legends.

Reporting summary

Further information on research design is available in the Nature Research Reporting Summary linked to this article.

Data availability

All raw data supporting the findings in Figs. 1–4 and Figs. S1-S4 of this study are available within the paper and its Supplementary Information and in Data S1-Data S2.

Code availability

Custom python scripts used for phylogenetic analysis are publicly available on GitHub: https://github.com/JonWinkelman/reciprocal-blast.

Received: 6 February 2025; Accepted: 3 June 2025;
Published online: 21 June 2025

References

1. Hudson, R. C. & Daniel, R. M. L-glutamate dehydrogenases: distribution, properties and mechanism. *Comp. Biochem Physiol. B*. **106**, 767–792 (1993).
2. Brunhuber, N. M. & Blanchard, J. S. The biochemistry and enzymology of amino acid dehydrogenases. *Crit. Rev. Biochem Mol. Biol.* **29**, 415–467 (1994).
3. Lázaro, M. et al. 3D architecture and structural flexibility revealed in the subfamily of large glutamate dehydrogenases by a mycobacterial enzyme. *Commun. Biol.* **4**, 684 (2021).
4. Miñambres, B., Olivera, E. R., Jensen, R. A. & Luengo, J. M. A new class of glutamate dehydrogenases (GDH). Biochemical and genetic characterization of the first member, the AMP-requiring NAD-specific GDH of *Streptomyces clavuligerus*. *J. Biol. Chem.* **275**, 39529–39542 (2000).
5. Commichau, F. M., Gunka, K., Landmann, J. J. & Stülke, J. Glutamate metabolism in *Bacillus subtilis*: gene expression and enzyme activities evolved to avoid futile cycles and to allow rapid responses to perturbations of the system. *J. Bacteriol.* **190**, 3557–3564 (2008).
6. Seah, S. Y. Industrial Enzymes: Structure, Function and Applications (Dordrecht: Springer Netherlands, 2007).
7. Adamson, H. et al. Rapid Quantification of *C. difficile* Glutamate Dehydrogenase and Toxin B (TcdB) with a NanoBiT Split-Luciferase Assay. *Anal. Chem.* **94**, 8156–8163 (2022).
8. DeMars, Z. & Bose, J. L. Redirection of Metabolism in Response to Fatty Acid Kinase in Staphylococcus aureus.*J Bacteriol*. **200**, e00345–18 (2018).
9. Halsey, C. R. et al. Amino Acid Catabolism in Staphylococcus aureus and the Function of Carbon Catabolite Repression. *mBio*. **8**, e01434–16 (2017).
10. Beaufay, F. et al. A NAD-dependent glutamate dehydrogenase coordinates metabolism with cell division in *Caulobacter crescentus*. *EMBO J.* **34**, 1786–1800 (2015).
11. Noda-García, L. et al. Chance and pleiotropy dominate genetic diversity in complex bacterial environments. *Nat. Microbiol.* **4**, 1221–1230 (2019).
12. Griffin, J. E. et al. High-resolution phenotypic profiling defines genes essential for mycobacterial growth and cholesterol catabolism. *PLoS Pathog.* **7**, e1002251 (2011).
13. Jayaraman, V. et al. A counter-enzyme complex regulates glutamate metabolism in *Bacillus subtilis*. *Nat. Chem. Biol.* **18**, 161–170 (2021).
14. Noda-Garcia, L., Romero Romero, M. L., Longo, L. M., Kolodkin-Gal, I. & Tawfik, D. S. Bacilli glutamate dehydrogenases diverged via coevolution of transcription and enzyme regulation. *EMBO Rep.* **18**, 1139–1149 (2017).
15. Girinathan, B. P., Braun, S., Sirigireddy, A. R., Lopez, J. E. & Govind, R. Importance of Glutamate Dehydrogenase (GDH) in *Clostridium difficile* Colonization In Vivo. *PLoS One* **11**, e0160107 (2016).
16. Chittick, L. & Okwumabua, O. Loss of expression of the glutamate dehydrogenase (gdh) of *Streptococcus suis* serotype 2 compromises growth and pathogenicity. *Micro. Pathog.* **188**, 106565 (2024).
17. Huang, X., Lao, W., Zhou, Y., Sun, Y. & Wang, Q. Glutamate dehydrogenase enables Salmonella to survive under oxidative stress and escape from clearance in macrophages. *FEBS Lett.* **596**, 81–94 (2022).
18. Gallant, J. L., Viljoen, A. J., van Helden, P. D. & Wiid, I. J. Glutamate Dehydrogenase Is Required by *Mycobacterium bovis* BCG for Resistance to Cellular Stress. *PLoS One* **11**, e0147706 (2016).
19. Gazioglu, O. et al. Glutamate Dehydrogenase (GdhA) of *Streptococcus pneumoniae* Is Required for High Temperature Adaptation. *Infect. Immun.* **89**, e0040021 (2021).
20. Lee, Y. H., Kingston, A. W. & Helmann, J. D. Glutamate dehydrogenase affects resistance to cell wall antibiotics in *Bacillus subtilis*. *J. Bacteriol.* **194**, 993–1001 (2012).
21. Tawfik, D. S. Enzyme promiscuity and evolution in light of cellular metabolism. *FEBS J.* **287**, 1260–1261 (2020).
22. Mathioudakis, L. et al. Localization of Human Glutamate Dehydrogenases Provides Insights into Their Metabolic Role and Their Involvement in Disease Processes. *Neurochem Res*. **44**, 170–187 (2019).
23. Belitsky, B. R. & Sonenshein, A. L. Role and regulation of *Bacillus subtilis* glutamate dehydrogenase genes. *J. Bacteriol.* **180**, 6298–6305 (1998).
24. Nye, T. M., Schroeder, J. W., Kearns, D. B. & Simmons, L. A. Complete Genome Sequence of Undomesticated *Bacillus subtilis* Strain NCIB 3610. *Genome Announc* **5** (2017).
25. Gunka, K. & Commichau, F. M. Control of glutamate homeostasis in *Bacillus subtilis*: a complex interplay between ammonium assimilation, glutamate biosynthesis and degradation. *Mol. Microbiol* **85**, 213–224 (2012).
26. Ranava, D. et al. Bidirectional sequestration between a bacterial hibernation factor and a glutamate metabolizing protein. *Proc. Natl Acad. Sci. USA* **119**, e2207257119 (2022).

27. Gunka, K. et al. Functional dissection of a trigger enzyme: mutations of the *Bacillus subtilis* glutamate dehydrogenase RocG that affect differentially its catalytic activity and regulatory properties. *J. Mol. Biol.* **400**, 815–827 (2010).
28. Vandooren, J., Geurts, N., Martens, E., Van den Steen, P. E. & Opdenakker, G. Zymography methods for visualizing hydrolytic enzymes. *Nat. Methods* **10**, 211–220 (2013).
29. Okwumabua, O., Persaud, J. S. & Reddy, P. G. Cloning and characterization of the gene encoding the glutamate dehydrogenase of *Streptococcus suis* serotype 2. *Clin. Diagn. Lab Immunol.* **8**, 251–257 (2001).
30. Warneke, R. et al. Ornithine is the central intermediate in the arginine degradative pathway and its regulation in *Bacillus subtilis*. *J. Biol. Chem.* **299**, 104944 (2023).
31. Debarbouille, M., Gardan, R., Arnaud, M. & Rapoport, G. Role of BkdR, a transcriptional activator of the SigL-dependent isoleucine and valine degradation pathway in Bacillus subtilis. *J. Bacteriol.* **181**, 2059–2066 (1999).
32. Kasu, I. R., Reyes-Matte, O., Bonive-Boscan, A., Derman, A. I. & Lopez-Garrido, J. Catabolism of germinant amino acids is required to prevent premature spore germination in *Bacillus subtilis*. *mBio* **15**, e0056224 (2024).
33. Baker, P. J., Turnbull, A. P., Sedelnikova, S. E., Stillman, T. J. & Rice, D. W. A role for quaternary structure in the substrate specificity of leucine dehydrogenase. *Structure* **3**, 693–705 (1995).
34. Gunka, K., Stannek, L., Care, R. A. & Commichau, F. M. Selection-driven accumulation of suppressor mutants in *Bacillus subtilis*: the apparent high mutation frequency of the cryptic *gudB* gene and the rapid clonal expansion of *gudB*(+) suppressors are due to growth under selection. *PLoS One* **8**, e66120 (2013).
35. Fullam, A. et al. proGenomes3: approaching one million accurately and consistently annotated high-quality prokaryotic genomes. *Nucleic Acids Res*. **51**, D760–D766 (2023).
36. Jumper, J. et al. Highly accurate protein structure prediction with AlphaFold. *Nature* **596**, 583–589 (2021).
37. Liu, J. et al. Metabolic co-dependence gives rise to collective oscillations within biofilms. *Nature* **523**, 550–554 (2015).
38. Bocci, F., Suzuki, Y., Lu, M. & Onuchic, J. N. Role of metabolic spatiotemporal dynamics in regulating biofilm colony expansion. *Proc. Natl Acad. Sci. USA* **115**, 4288–4293 (2018).
39. Kimura, T. & Kobayashi, K. Role of Glutamate Synthase in Biofilm Formation by *Bacillus subtilis*. *J. Bacteriol.* **202**, e00120–e00120 (2020).
40. Shemesh, M. & Chai, Y. A combination of glycerol and manganese promotes biofilm formation in *Bacillus subtilis* via histidine kinase KinD signaling. *J. Bacteriol.* **195**, 2747–2754 (2013).
41. Vlamakis, H., Chai, Y., Beauregard, P., Losick, R. & Kolter, R. Sticking together: building a biofilm the *Bacillus subtilis* way. *Nat. Rev. Microbiol* **11**, 157–168 (2013).
42. Gunka, K. et al. A high-frequency mutation in *Bacillus subtilis*: requirements for the decryptification of the *gudB* glutamate dehydrogenase gene. *J. Bacteriol.* **194**, 1036–1044 (2012).
43. Flórez, L. A., Gunka, K., Polanía, R., Tholen, S. & Stülke, J. SPABBATS: A pathway-discovery method based on Boolean satisfiability that facilitates the characterization of suppressor mutants. *BMC Syst. Biol.* **5**, 5 (2011).
44. Bennett, B. D. et al. Absolute metabolite concentrations and implied enzyme active site occupancy in *Escherichia coli*. *Nat. Chem. Biol.* **5**, 593–599 (2009).
45. Young, V. R. & Ajami, A. M. Glutamate: an amino acid of particular distinction. *J. Nutr.* **130**, 892S–900S (2000).
46. Oh, Y. K., Palsson, B. O., Park, S. M., Schilling, C. H. & Mahadevan, R. Genome-scale reconstruction of metabolic network in *Bacillus subtilis* based on high-throughput phenotyping and gene essentiality data. *J. Biol. Chem.* **282**, 28791–28799 (2007).
47. Krüger, L. et al. Essentiality of c-di-AMP in *Bacillus subtilis*: Bypassing mutations converge in potassium and glutamate homeostasis. *PLoS Genet* **17**, e1009092 (2021).
48. Stannek, L. et al. Evidence for synergistic control of glutamate biosynthesis by glutamate dehydrogenases and glutamate in *Bacillus subtilis*. *Environ. Microbiol* **17**, 3379–3390 (2015).
49. Calogero, S. et al. RocR, a novel regulatory protein controlling arginine utilization in Bacillus subtilis, belongs to the NtrC/NifA family of transcriptional activators. *J. Bacteriol.* **176**, 1234–1241 (1994).
50. Commichau, F. M., Herzberg, C., Tripal, P., Valerius, O. & Stülke, J. A regulatory protein-protein interaction governs glutamate biosynthesis in *Bacillus subtilis*: the glutamate dehydrogenase RocG moonlights in controlling the transcription factor GltC. *Mol. Microbiol* **65**, 642–654 (2007).
51. Commichau, F. M. & Stülke, J. Trigger enzymes: bifunctional proteins active in metabolism and in controlling gene expression. *Mol. Microbiol* **67**, 692–702 (2008).
52. Turnbull, A. P., Baker, P. J. & Rice, D. W. Analysis of the quaternary structure, substrate specificity, and catalytic mechanism of valine dehydrogenase. *J. Biol. Chem.* **272**, 25105–25111 (1997).
53. Wang, X. G., Britton, K. L., Stillman, T. J., Rice, D. W. & Engel, P. C. Conversion of a glutamate dehydrogenase into methionine/norleucine dehydrogenase by site-directed mutagenesis. *Eur. J. Biochem* **268**, 5791–5799 (2001).
54. Stillman, T. J. et al. Insights into the mechanism of domain closure and substrate specificity of glutamate dehydrogenase from *Clostridium symbiosum*. *J. Mol. Biol.* **285**, 875–885 (1999).
55. Sun, Y. et al. Acetylation coordinates the crosstalk between carbon metabolism and ammonium assimilation in *Salmonella enterica*. *EMBO J.* **42**, e112333 (2023).
56. Chou, K. T. et al. A segmentation clock patterns cellular differentiation in a bacterial biofilm. *Cell* **185**, 145–157.e113 (2022).
57. Tran, P., Lander, S. M. & Prindle, A. Active pH regulation facilitates *Bacillus subtilis* biofilm development in a minimally buffered environment. *mBio* **15**, e0338723 (2024).
58. Arnaouteli, S., Bamford, N. C., Stanley-Wall, N. R. & Kovács, ÁT. *Bacillus subtilis* biofilm formation and social interactions. *Nat. Rev. Microbiol* **19**, 600–614 (2021).
59. Kesel, S. et al. Direct Comparison of Physical Properties of *Bacillus subtilis* NCIB 3610 and B-1 Biofilms. *Appl Environ. Microbiol* **82**, 2424–2432 (2016).
60. Schneewind, O. & Missiakas, D. Genetic manipulation of *Staphylococcus aureus*. *Curr. Protoc. Microbiol.* **32**, Unit 9C 3 (2014).
61. Bruckner, R. A series of shuttle vectors for *Bacillus subtilis* and *Escherichia coli*. *Gene* **122**, 187–192 (1992).
62. Fuller, J. R. et al. Identification of a lactate-quinone oxidoreductase in *Staphylococcus aureus* that is essential for virulence. *Front Cell Infect. Microbiol* **1**, 19 (2011).
63. Unger, T., Jacobovitch, Y., Dantes, A., Bernheim, R. & Peleg, Y. Applications of the Restriction Free (RF) cloning procedure for molecular manipulations and protein expression. *J. Struct. Biol.* **172**, 34–44 (2010).
64. Branda, S. S., González-Pastor, J. E., Ben-Yehuda, S., Losick, R. & Kolter, R. Fruiting body formation by *Bacillus subtilis*. *Proc. Natl Acad. Sci. USA* **98**, 11621–11626 (2001).
65. Koo, B. M. et al. Construction and Analysis of Two Genome-Scale Deletion Libraries for *Bacillus subtilis*. *Cell Syst.* **4**, 291–305.e297 (2017).
66. Yasbin, R. E. & Young, F. E. Transduction in *Bacillus subtilis* by bacteriophage SPP1. *J. Virol.* **14**, 1343–1348 (1974).
67. Kearns, D. B., Chu, F., Branda, S. S., Kolter, R. & Losick, R. A master regulator for biofilm formation by *Bacillus subtilis*. *Mol. Microbiol* **55**, 739–749 (2005).
68. Konkol, M. A., Blair, K. M. & Kearns, D. B. Plasmid-encoded ComI inhibits competence in the ancestral 3610 strain of *Bacillus subtilis*. *J. Bacteriol.* **195**, 4085–4093 (2013).

69. Lander, S. M., Fisher, G., Everett, B. A., Tran, P. & Prindle, A. Secreted nucleases reclaim extracellular DNA during biofilm development. *NPJ Biofilms Microbiomes* **10**, 103 (2024).
70. Lipońska, A., Lee, H. & Yap, M. F. Staphylococcal exoribonuclease YhaM destabilizes ribosomes by targeting the mRNA of a hibernation factor. *Nucleic Acids Res*. **52**, 8998–9013 (2024).
71. Yap, M. N. & Bernstein, H. D. Mutations in the *Escherichia coli* ribosomal protein L22 selectively suppress the expression of a secreted bacterial virulence factor. *J. Bacteriol.* **195**, 2991–2999 (2013).
72. Emms, D. M. & Kelly, S. OrthoFinder: phylogenetic orthology inference for comparative genomics. *Genome Biol.* **20**, 238 (2019).
73. Abramson, J. et al. Accurate structure prediction of biomolecular interactions with AlphaFold 3. *Nature* **630**, 493–500 (2024).
74. Holm, L. Using Dali for Protein Structure Comparison. *Methods Mol. Biol.* **2112**, 29–42 (2020).
75. Mhatre, E. et al. The impact of manganese on biofilm development of *Bacillus subtilis*. *Microbiology* **162**, 1468–1478 (2016).

Acknowledgements

We thank Jeffrey Bose for advice on *gudB* mutant complementation, Fitnat Yilidz for comments on biofilm experiments, the late Dan Tawfik for a generous gift of *B. subtilis* GudB antibody, and Vijay Jayaraman for feedback on GudB oligomerization. This work was supported by National Institutes of Health (NIH) grants R01GM121359, R01AI150986, and the Northwestern University Faculty Startup Fund (to MFY). A.P. received generous support from the National Science Foundation (NSF 2239567), NIH (R35GM147170), Pew Charitable Trusts (2019-A-06953), the Army Research office (W911NF-19-1-0136), and the David and Lucile Packard Foundation (2018-68055). S.M.L. was supported by an NIH predoctoral fellowship F31GM143907. Transposon mutants were obtained through Network on Antimicrobial Resistance in Staphylococcus aureus (NARSA) for distribution by BEI Resources, NIAID, NIH.

Author contributions

D.R.—Conceptualization, investigation, validation, formal analysis, writing. S.M.L., S.Y.K.—Investigation, validation.JDW- Formal analysis, software, visualization. A.P.—Resources, funding acquisition, supervision. M.F.Y.—Conceptualization, project administration, investigation, funding acquisition, supervision, writing. D.R., S.M.L., S.Y.K., J.D.W., A.P., M.F.Y.—Review, edit and approve the manuscript.

Competing interests

The authors declare no competing interests.

Additional information

Supplementary information The online version contains supplementary material available at https://doi.org/10.1038/s41522-025-00750-6.

Correspondence and requests for materials should be addressed to David Ranava or Mee-Ngan F. Yap.